

# Numerical Heat Transfer, Part A: Applications

## An International Journal of Computation and Methodology

ISSN: (Print) (Online) Journal homepage: <https://www.tandfonline.com/loi/unht20>

---

# Computational analysis of entropy generation in three-dimensional mixed convection flow with thermal dissipation and variable thermal conductivity

Muhammad Idrees Afridi, Muhammad Qasim & Ali J. Chamkha

**To cite this article:** Muhammad Idrees Afridi, Muhammad Qasim & Ali J. Chamkha (20 Nov 2023): Computational analysis of entropy generation in three-dimensional mixed convection flow with thermal dissipation and variable thermal conductivity, Numerical Heat Transfer, Part A: Applications, DOI: [10.1080/10407782.2023.2282150](https://doi.org/10.1080/10407782.2023.2282150)

**To link to this article:** <https://doi.org/10.1080/10407782.2023.2282150>



Published online: 20 Nov 2023.



Submit your article to this journal [↗](#)





View related articles [↗](#)



View Crossmark data [↗](#)



# Computational analysis of entropy generation in three-dimensional mixed convection flow with thermal dissipation and variable thermal conductivity

Muhammad Idrees Afridi<sup>a</sup> , Muhammad Qasim<sup>b</sup>, and Ali J. Chamkha<sup>c</sup> 

<sup>a</sup>School of Mathematics and Computer Science, Hanjiang Normal University, Shiyao, P.R. China; <sup>b</sup>Department of Mathematics, COMSATS University Islamabad (CUI), Islamabad, Pakistan; <sup>c</sup>Faculty of Engineering, Kuwait College of Science and Technology, Kuwait City, Kuwait

## ABSTRACT

Entropy generation in steady three-dimensional thermal flow is investigated under the coupled influence of viscous dissipation and mixed convection. The stretching sheet with an exponential velocity profile induces the flow. In this examination, we presume that the fluid is incompressible and possesses a Newtonian behavior and temperature-dependent thermal conductivity. Using the appropriate classical similarity variables reduces the dimensional nonlinear dynamical system of governing equations to a dimensionless nonlinear dynamical set of ordinary differential equations. It's important to note that the selection of an exponentially varying surface temperature is deliberate, as it enables precise similarity transformations to be established in situations involving both viscous dissipation and buoyancy forces. The simplified finite difference approach (SFDM) is used to solve the acquired nonlinear dynamical set of ordinary differential equations. The tridiagonal matrix approach is used to solve the resulting system of algebraic equations. In a particular situation, the present numerical simulation is numerically checked with the previously available results and observed a good agreement. The effects of physical parameters on velocity, temperature, surface stresses and heat transfer rate, entropy generation, and the irreversibility parameter are investigated. The entropy generation rate exhibits a decreasing trend with respect to the mixed convection parameter in the vicinity of the stretching surface. Entropy reduction can be achieved by employing a working fluid with a low Prandtl number and by minimizing the fluid friction.

## ARTICLE HISTORY

Received 13 April 2023  
Revised 15 September 2023  
Accepted 23 October 2023

## KEYWORDS

Bejan Number; entropy generation minimization (EGM); finite difference method (FDM); mixed convection; variable thermal conductivity; viscous dissipation

## 1. Introduction

Thermal systems are encountered in various branches of engineering, from mechanical to biomedical. Among them are heat exchangers, cooling devices, energy storage systems, power generation plants, renewable energy systems, heat pumps, cryosurgical instruments, ventricular assist devices and electroosmotic pumps. The energy loss caused by thermodynamic irreversibility is undesirable because it reduces the ability to work and is quantified as entropy. The generation of entropy in a thermal system has a direct impact on its feasibility and efficiency. Therefore, it is vital to identify irreversible sources in components and systems. Bejan [1, 2] introduced an optimization tool as the fundamentals of entropy generation minimization. This technique based on

### Nomenclature

$Be$	Bejan number	$\alpha$	Stretching ratio parameter
$c_p$	Specific heat	$\beta_T^*$	Thermal expansion coefficient
$Ec$	Eckert number	$\lambda$	Mixed convection parameter
$\dot{E}_G'''$	Volumetric entropy generation rate	$\Lambda$	Temperature difference parameter
$g$	Gravitational acceleration	$\tau$	Variable thermal conductivity parameter
$k$	Thermal conductivity	$\rho$	Fluid density
$N_G$	Entropy generation number	$\mu$	Dynamic viscosity
$Pr$	Prandtl number	$\nu$	Kinematic viscosity
$T^*$	Temperature field	$\xi$	Similarity variable
$u^*, v^*, w^*$	Velocity components	$\Theta$	Dimensionless temperature
$x^*, y^*, z^*$	Spatial Coordinates		

the second law of thermodynamics is now being widely used in optimizing and evaluating the performance of thermal systems. Several numerical and analytical studies on entropy generation in various configurations and physical processes have been published in the literature [3–12].

The Navier-Stokes equations are nonlinear elliptic partial differential equations and are difficult to study except for a few cases where they have an exact solution. In the boundary layer flows, under boundary layer approximation, several terms become negligible inside the thin region, and the Navier-Stokes equation transforms from elliptic to parabolic. Numerous practical applications necessitate close attention to flow behavior. For example, in the design and analysis of the drag in aircraft, submarines, jet engines, rockets, wake and separation of boundary layers, continuous casting, and development of boundary layer along with thin films in condensation processes. Apart from that, more useful features can be found in heat transfer mechanisms, mixing enhancement, cooling of electronic components, geothermal power generation, cooling of continuous filaments, species transport, and so on [13–20]. Further, there are numerous industrial and manufacturing applications for boundary layer flows such as fiberglass, papermaking and castings and cooling processes for alloys such as steel or aluminum.

Several analytical, numerical and hybrid techniques are developed to compute the solutions of the boundary layer equations [21–30]. One approach for solving corresponding boundary layer problems is the local similarity method. One of the primary advantages of this technique is that no values at upstream locations are required to compute the value at a particular stream-wise location. Additionally, this approach has the advantage of converting transport partial differential equations (PDEs) into ordinary differential equations (ODEs) *via* suitable local self-similarity variables [31–35]. The self-similar equations for boundary layer flow over-stretching sheets are not always achievable as it strongly depends on the choice of stretching, free stream velocities, the form of the surface temperature and many other factors. For example, for the constant surface temperature case, self-similar solutions for boundary layer flows in the presence of viscous dissipation and mixed convection flows are not possible and the choice of variable surface temperature is related to the form of stretching velocity [36–40].

Partha et al. [41] for the first time established a self-similar solution for two-dimensional mixed convection flow caused by an exponentially stretched surface with frictional heating by choosing a special type of surface temperature and assured that both the mixed convection parameter and Eckert numbers are independent of the spatial variables. Effects of thermal radiation and viscous dissipation on the boundary layer flow across an exponentially stretching sheet are also reported by Bidin and Nazar [42]. They transformed the governing equations into a self-similar form by choosing the variable surface temperature that facilitates the similarity transformation in a way that the Eckert number is independent of the space variable. Afridi et al. [43] conducted an entropy generation analysis of the flow generated by an exponentially stretching sheet having temperature-dependent viscosity and thermal conductivity. In another attempt,

Qasim and Afridi [44] investigated the entropy production in the two-dimensional mixed convection flow in the presence of viscous dissipation. Appropriate transformations are utilized to convert fundamental governing PDEs into nonlinear ODEs. Liu et al. [45] investigated the three-dimensional flow of a viscous fluid over an exponentially stretched sheet for the first time and introduced a new similarity transformation. Afridi and Qasim [46] extended the analysis of Liu et al. [45] to explore the heat transfer characteristics as well as scrutinized the entropy generation in the presence of viscous dissipation and computed the similarity solutions.

This study aims to report a self-similar solution of the mixed convective three-dimensional boundary layer flows over an exponentially stretched sheet by incorporating viscous dissipation. Moreover, the thermal conductivity of the fluid is considered temperature-dependent. Second law analysis is also performed to explore the effect of various physical parameters on the minimization of entropy. Opting for a special type of surface temperature that enables the similarity transformations to transform the boundary layer equations into self-similar non-linear ordinary differential equations, which are solved numerically using the simplified finite difference method (SFDM) along with the tridiagonal matrix algorithm (TDMA) [47, 48]. A comparison of current and previous limiting results is also performed to ensure that the proposed numerical scheme is accurate.

## 2. The mathematical model

Consider a bi-directional stretching surface causing mixed convection flow in three dimensions. The fluid is assumed incompressible having a variable (temperature-dependent) thermal conductivity. Fluid flowing outside the boundary layer and the surface of the stretching sheet are kept at the temperature  $T_b^*$  and  $T_w^*$  respectively and further it is assumed that  $T_w^* > T_b^*$ . Figure 1(a) shows the configuration of flow and coordinates the system

The flow under consideration has the following governing equations:

$$\frac{\partial u^*}{\partial x^*} + \frac{\partial v^*}{\partial y^*} + \frac{\partial w^*}{\partial z^*} = 0, \quad (1)$$

$$u^* \frac{\partial u^*}{\partial x^*} + v^* \frac{\partial u^*}{\partial y^*} + w^* \frac{\partial u^*}{\partial z^*} - \nu \frac{\partial^2 u^*}{\partial z^{*2}} - g\beta_T^*(T^* - T_b^*) = 0, \quad (2)$$

$$u^* \frac{\partial v^*}{\partial x^*} + v^* \frac{\partial v^*}{\partial y^*} + w^* \frac{\partial v^*}{\partial z^*} - \nu \frac{\partial^2 v^*}{\partial z^{*2}} = 0, \quad (3)$$

$$\rho c_p \left[ u^* \frac{\partial T^*}{\partial x^*} + v^* \frac{\partial T^*}{\partial y^*} + w^* \frac{\partial T^*}{\partial z^*} \right] - k(T^*) \frac{\partial^2 T^*}{\partial z^{*2}} - \left( \frac{\partial T^*}{\partial z^*} \right)^2 \frac{\partial k(T^*)}{\partial T^*} - \mu \left[ \left( \frac{\partial u^*}{\partial z^*} \right)^2 + \left( \frac{\partial v^*}{\partial z^*} \right)^2 \right] = 0. \quad (4)$$

The dimensional no-slip conditions for velocity and temperature are

$$\left. \begin{aligned} u^* = u_w^* = u_0^* e^{\frac{x^*+y^*}{L}}, v^* = v_w^* = v_0^* e^{\frac{x^*+y^*}{L}}, w^* = 0 \text{ at } z^* = 0, \\ T^* = T_w^* = T_b^* + T_0^* e^{2\left(\frac{x^*+y^*}{L}\right)} \text{ at } z^* = 0, \\ u^* \rightarrow 0, v^* \rightarrow 0, T^* \rightarrow T_b^*, \text{ as } z^* \rightarrow \infty \end{aligned} \right\}. \quad (5)$$

The change in thermal conductivity with temperature is described as given below

$$k(T^*) = k_b \left( 1 + \tau \frac{T^* - T_b^*}{T_w^* - T_b^*} \right). \quad (6)$$

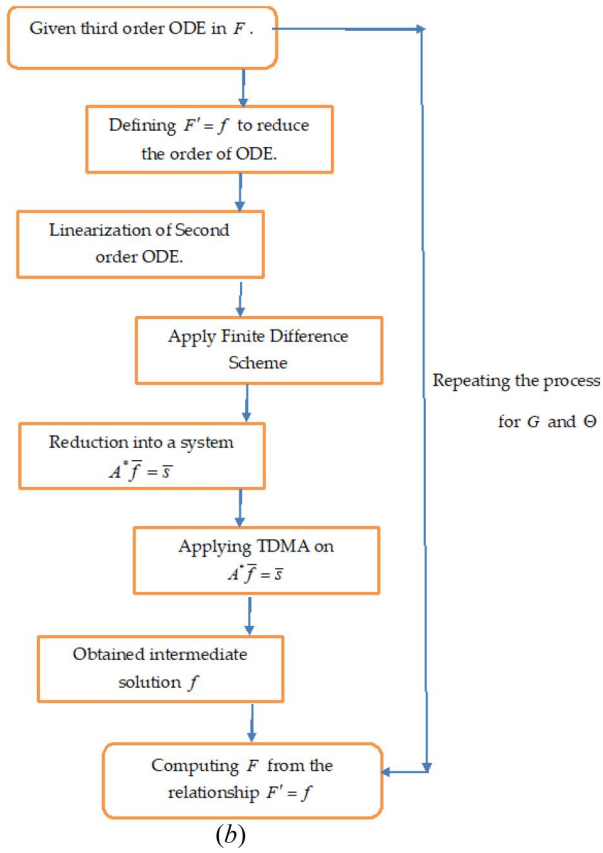
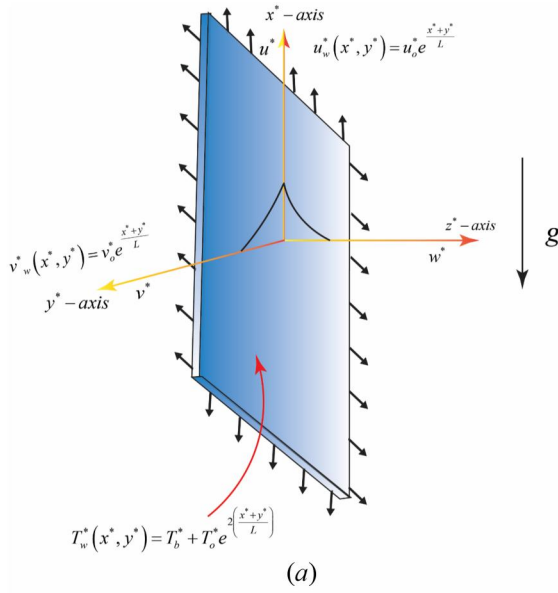


Figure 1. (a) Configuration of flow and the coordinate system. (b) Flow diagram for the applied numerical scheme.

Here  $\langle u^*, v^*, w^* \rangle$  shows velocity components along with  $\langle x^*, y^*, z^* \rangle$  directions,  $\mu$  is dynamic viscosity,  $\rho$  is density,  $k(T^*)$  shows variable thermal conductivity,  $\tau$  is variable thermal conductivity parameter,  $k_b$  represent thermal conductivity at  $T^* = T_b^*$ ,  $g$  means gravitational acceleration,  $\beta_T^*$  shows an expansion of thermal coefficient,  $T^*$  is the dimensional temperature,  $c_p$  represents specific heat,  $\langle u_0^*, v_0^* \rangle$ ,  $L$  and  $T_0^*$  respectively, represents the characteristic velocities, length, and temperature.

Invoking the transformations

$$\left. \begin{aligned} \zeta &= \sqrt{\frac{u_0^*}{2\nu L}} z^* \exp\left(\frac{x^* + y^*}{2L}\right), u^* = u_0^* \exp\left(\frac{x^* + y^*}{L}\right) \frac{dF}{d\xi}, v^* = u_0^* \exp\left(\frac{x^* + y^*}{L}\right) \frac{dG}{d\xi} \\ w^* &= -\sqrt{\frac{\nu u_0^*}{2L}} e^{\left(\frac{x^* + y^*}{2L}\right)} (F + \zeta F' + G + \zeta G'), T^* = \Theta(T_w^* - T_b^*) + T_b^* \end{aligned} \right\}, \quad (7)$$

The dimensional equations (2)-(4) reduce to the following forms

$$\frac{d^3 F}{d\xi^3} + \frac{d^2 F}{d\xi^2} (F + G) - 2 \frac{dF}{d\xi} \left[ \frac{dF}{d\xi} + \frac{dG}{d\xi} \right] + 2\lambda\Theta = 0, \quad (8)$$

$$\frac{d^3 G}{d\xi^3} + \frac{d^2 G}{d\xi^2} (F + G) - 2 \frac{dG}{d\xi} \left[ \frac{dF}{d\xi} + \frac{dG}{d\xi} \right] = 0, \quad (9)$$

$$\left. \begin{aligned} [1 + \Theta\tau] \frac{d^2 \Theta}{d\xi^2} + \tau \left( \frac{d\Theta}{d\xi} \right)^2 + \text{Pr} \frac{d\Theta}{d\xi} (F + G) \\ - 4\text{Pr}\Theta \left[ \frac{dF}{d\xi} + \frac{dG}{d\xi} \right] + \text{EcPr} \left[ \left( \frac{d^2 F}{d\xi^2} \right)^2 + \left( \frac{d^2 G}{d\xi^2} \right)^2 \right] = 0 \end{aligned} \right\}. \quad (10)$$

Whereas the diemnsional boundary conditions (5), can be written in dimensionless form as given below

$$\left. \begin{aligned} F(0) = 0, \left. \frac{dG}{d\xi} \right|_{\xi=0} = \alpha, \left. \frac{dF}{d\xi} \right|_{\xi=0} = 1, G(0) = 0, \Theta(0) = 1, \\ \left. \frac{dF}{d\xi} \right|_{\xi \rightarrow \infty} = \left. \frac{dG}{d\xi} \right|_{\xi \rightarrow \infty} = \Theta(\xi \rightarrow \infty) \rightarrow 0, \end{aligned} \right\}. \quad (11)$$

Where  $\alpha = \frac{v_0^*}{u_0^*}$  (stretching ratio parameter),  $\lambda = \frac{g\beta_T^* T_0^* L}{u_0^{*2}}$  (mixed convection parameter)  $\text{Ec} = \frac{u_0^{*2}}{c_p T_0^*}$  (Eckert number) and  $\text{Pr} = \frac{\mu c_p}{k_b}$  (Prandtl number).

### 3. Entropy generation

Entropy generation (production),  $\dot{E}_G'''$ , in three-dimensional boundary layer flows by considering variable thermal conductivity and incorporating viscous dissipation, can be described as:

$$\dot{E}_G''' = \frac{1}{T^*} \left[ \frac{k(T^*)}{T^*} (\nabla T^*)^2 + \mu \Pi \right]. \quad (12)$$

Where  $\nabla T^*$  (temperature gradient) and  $\Pi$  (dissipation function) in a three-dimension coordinate system take the following form

$$\nabla T^* = \left( \frac{\partial T^*}{\partial x^*}, \frac{\partial T^*}{\partial y^*}, \frac{\partial T^*}{\partial z^*} \right), \quad (13)$$

$$\Pi = 2 \left[ \left( \frac{\partial u^*}{\partial x^*} \right)^2 + \left( \frac{\partial v^*}{\partial y^*} \right)^2 + \left( \frac{\partial w^*}{\partial z^*} \right)^2 \right] + \left( \frac{\partial u^*}{\partial y^*} + \frac{\partial u^*}{\partial x^*} \right)^2 + \left( \frac{\partial v^*}{\partial z^*} + \frac{\partial w^*}{\partial y^*} \right)^2 + \left( \frac{\partial w^*}{\partial x^*} + \frac{\partial u^*}{\partial z^*} \right)^2. \quad (14)$$

Substituting equations (13) and (14) in equation (12) and utilizing the boundary layer approximations, we have

$$\dot{E}_G''' = \frac{k(T^*)}{T^{*2}} \left( \frac{\partial T^*}{\partial z^*} \right)^2 + \frac{\mu}{T^*} \left[ \left( \frac{\partial u^*}{\partial z^*} \right)^2 + \left( \frac{\partial v^*}{\partial z^*} \right)^2 \right]. \quad (15)$$

After utilizing the transformations (7), Equation (15) reduce to

$$N_G(\xi) = \frac{\dot{E}_G'''}{(\dot{E}''')_c} = \frac{1}{(\Theta + \Lambda)} \left[ \frac{(1 + \tau\Theta)}{(\Theta + \Lambda)} \left( \frac{d\Theta}{d\xi} \right)^2 + EcPr \left( \left( \frac{d^2F}{d\xi^2} \right)^2 + \left( \frac{d^2G}{d\xi^2} \right)^2 \right) \right]. \quad (16)$$

Here,  $N_G = \frac{\dot{E}_G'''}{(\dot{E}''')_c}$  is dimensionless entropy generation,  $(\dot{E}''')_c = \frac{k_b u_w^*}{2\nu L}$  is characteristic entropy and  $\Lambda = \frac{T_b^*}{T_w^* - T_b^*}$  is a temperature difference parameter.

The Bejan number ( $Be$ ) describes how heat transfer affects entropy generation relative to other sources and is described by

$$Be = \frac{\frac{k(T^*)}{T^{*2}} \left( \frac{\partial T^*}{\partial z^*} \right)^2 \rightarrow \text{thermal effect}}{\underbrace{\frac{k(T^*)}{T^{*2}} \left( \frac{\partial T^*}{\partial z^*} \right)^2}_{\text{thermal effect}} + \underbrace{\frac{\mu}{T^*} \left[ \left( \frac{\partial u^*}{\partial z^*} \right)^2 + \left( \frac{\partial v^*}{\partial z^*} \right)^2 \right]}_{\text{viscous dissipation effect}}}. \quad (17)$$

Bejan number in terms of dimensionless variables is obtained by using equation (7) as given below

$$Be(\xi) = \frac{(1 + \Theta\tau) \left( \frac{d\Theta}{d\xi} \right)^2}{(1 + \Theta\tau) \left( \frac{d\Theta}{d\xi} \right)^2 + EcPr \left( \left( \frac{d^2F}{d\xi^2} \right)^2 + \left( \frac{d^2G}{d\xi^2} \right)^2 \right) (\Theta + \Lambda)}. \quad (18)$$

#### 4. Solution methodology

Constructing a closed-form solution for the resultant set of nonlinear ordinary differential equations (8)-(11) is not feasible. As a result, it is generally advisable to resort to numerical solutions for addressing such physical problems, utilizing advanced and accurate numerical techniques for optimal results. One of them is the ‘‘simplified finite difference method’’ proposed by Na [47]. The following are the main steps of this technique (also see the flow chart Figure 1b):

1. The third-order ODE is re-written as a system of first- and second-order ODEs.
2. Linearized the second-order ODE using Taylor’s series expansion.
3. The obtained linear second-order ODE is discretized using finite differences to get an algebraic system.
4. TDMA is utilized to solve the system of algebraic equations.

In our study, the thickness of the boundary layer (the length of the computational domain)  $\xi_\infty = 8$  seems to be sufficient to obtain a solution with asymptotically satisfying boundary conditions. In order to convert Eqs. (8) and (9) into first and second order ODE systems, we assume that

$$f = \frac{dF}{d\xi}, \quad (19)$$

$$g = \frac{dG}{d\xi}, \quad (20)$$

Invoking these, Eqs. (8) and (9) respectively, reduced to the following forms

$$\frac{d^2f}{d\xi^2} = 2f[f + g] - \frac{df}{d\xi}(F + G) - 2\lambda\Theta, \quad (21)$$

$$\frac{d^2g}{d\xi^2} = 2g[f + g] - \frac{dg}{d\xi}(F + G). \quad (22)$$

From Equation (21) and (22), we define two new variables

$$\chi_1 \left( \xi, f, \frac{df}{d\xi} \right) = 2f[f + g] - \frac{df}{d\xi}(F + G) - 2\lambda\Theta, \quad (23)$$

$$\chi_2 \left( \xi, g, \frac{dg}{d\xi} \right) = g[f + g] - \frac{dg}{d\xi}(F + G), \quad (24)$$

The linearized equation for  $f(\xi)$  and  $g(\xi)$  are respectively given by

$$f''_{n+1} + A_n f'_{n+1} + B_n f_{n+1} = D_n, \quad (25)$$

$$g''_{n+1} + \widehat{A}_n g'_{n+1} + \widehat{B}_n g_{n+1} = \widehat{D}_n, \quad (26)$$

The coefficients are written as follows:

$$\left. \begin{aligned} A_n &= - \left( \frac{\partial \chi_1}{\partial f'} \right)_n = F_n + G_n \\ B_n &= - \left( \frac{\partial \chi_1}{\partial f} \right)_n = -2[2f_n + g_n] \\ C_n &= \chi_1 \left( \xi, f, \frac{df}{d\xi} \right) - \left( \frac{\partial \chi_1}{\partial f} \right)_n f_n - \left( \frac{\partial \chi_1}{\partial f'} \right)_n f'_n \end{aligned} \right\}, \quad (27)$$

$$\left. \begin{aligned} \widehat{A}_n &= - \left( \frac{\partial \chi_2}{\partial g'} \right)_n = F_n + G_n \\ \widehat{B}_n &= - \left( \frac{\partial \chi_2}{\partial g} \right)_n = -2[f_n + 2g_n] \\ \widehat{C}_n &= \chi_2 \left( \xi, g, \frac{dg}{d\xi} \right) - \left( \frac{\partial \chi_2}{\partial g} \right)_n g_n - \left( \frac{\partial \chi_2}{\partial g'} \right)_n g'_n \end{aligned} \right\}. \quad (28)$$

Similarly, the linearized form of energy equation (10) is expressed by

$$\Theta''_{n+1} + P_n(\xi, \Theta_n, \Theta'_n) \Theta'_{n+1} + Q_n(\xi, \Theta_n, \Theta'_n) \Theta_{n+1} = R_n(\xi, \Theta_n, \Theta'_n). \quad (31)$$

The new variable  $\chi_3\left(\xi, \Theta, \frac{d\Theta}{d\xi}\right)$  and the coefficients are defined by

$$\chi_3\left(\xi, \Theta, \frac{d\Theta}{d\xi}\right) = (1 + \tau\Theta)^{-1} \left\{ \begin{array}{l} 4\Pr\Theta[f + g] \\ -\tau\left(\frac{d\Theta}{d\xi}\right)^2 - \Pr\frac{d\Theta}{d\xi}(F + G) \\ -Ec\Pr\left[\left(\frac{df}{d\xi}\right)^2 + \left(\frac{dg}{d\xi}\right)^2\right] \end{array} \right\}, \quad (32)$$

$$\left. \begin{array}{l} P_n = -\left(\frac{\partial\chi_3}{\partial\Theta'}\right)_n = \frac{2\tau\Theta'_n}{1 + \tau\Theta_n} + \frac{\Pr(F_n + G_n)}{1 + \tau\Theta_n}, \\ Q_n = -\left(\frac{\partial\chi_3}{\partial\Theta}\right)_n = -\frac{1}{(1 + \tau\Theta_n)^2} \left[ \tau^2(\Theta'^2)_n + \tau\Pr\Theta'_n(F_n + G_n) + \right. \\ \left. R_n = \chi_3(\xi, \Theta_n, \Theta'_n) + P_n\Theta'_n + Q_n\Theta_n. \right] \end{array} \right\} \quad (33)$$

As a result of applying the second-order central difference approximation to the derivatives, Eqs. (23) and (25) have the following discrete form:

$$\chi_1\left(\xi_j, f_j, \frac{df}{d\xi}\bigg|_j\right) = 2f_j[f_j + g_j] - \left(\frac{f_{j+1} - f_{j-1}}{2h}\right)(F_j + G_j) - 2\lambda\Theta_j, \quad (34)$$

$$\left(\frac{f_{j-1} - 2f_j + f_{j+1}}{h^2}\right)_{n+1} + (A_j)_n \left(\frac{f_{j+1} - f_{j-1}}{2h}\right)_{n+1} + (B_j)_n (f_j)_{n+1} = (D_j)_n. \quad (35)$$

Where  $j = 2$  to  $N$  and represent the interior nodes, the subscript  $n$  shows the previous iteration and the discretized form of the coefficients are as follows:

$$\left. \begin{array}{l} (A_j)_n = (F_j)_n + (G_j)_n \\ (B_j)_n = -2\left[2(f_j)_n + (g_j)_n\right] \\ (C_j)_n = \chi_1\left(\xi_j, f_j, \frac{df}{d\xi}\bigg|_j\right) + (B_j)_n f_n + (A_j)_n \left(\frac{f_{j+1} - f_{j-1}}{2h}\right) \end{array} \right\}. \quad (36)$$

Here  $h$  represent the size of the interval and is constant throughout the simulation because of the uniform discretization.

After some simplification, Equation (35) becomes

$$\bar{a}_j(f_{j-1})_{n+1} + \bar{b}_j(f_j)_{n+1} + \bar{c}_j(f_{j+1})_{n+1} = \bar{d}_j, \quad j = 1, 2, 3, \dots, N, \quad (37)$$

here

$$\left. \begin{array}{l} \bar{a}_j = 2 - h(A_j)_n \\ \bar{b}_j = -4 + 2h^2(B_j)_n \\ \bar{c}_j = 2 + h(A_j)_n \\ \bar{d}_j = 2h^2(D_j)_n \end{array} \right\}. \quad (38)$$

The boundary conditions in finite difference notations are

$$\left. \begin{array}{l} f_{j=1} = f_0 = 1 \\ f_{j=N} = f_N = 0 \end{array} \right\}, \quad (39)$$

Equation (37) is a system of  $(N - 1)$  algebraic equations, which in the matrix-vector form are as follows

$$A^* \bar{f} = \bar{s}. \quad (40)$$

Where,

$$\left. \begin{aligned} A^* &= \begin{pmatrix} \bar{b}_1 & \bar{c}_1 & 0 & & 0 \\ \bar{a}_2 & \bar{b}_2 & \bar{c}_2 & & 0 \\ 0 & \bar{a}_3 & \bar{b}_3 & \cdots & 0 \\ & \vdots & & \ddots & \vdots \\ 0 & 0 & 0 & \cdots & \bar{b}_{N-1} \end{pmatrix} \\ \bar{f} &= \begin{pmatrix} f_1 \\ f_2 \\ f_3 \\ \vdots \\ f_{N-1} \end{pmatrix}^{n+1} \\ \bar{s} &= \begin{pmatrix} \bar{s}_1 \\ \bar{s}_2 \\ \bar{s}_3 \\ \vdots \\ \bar{s}_{N-1} \end{pmatrix} = \begin{pmatrix} \bar{d}_1 - \bar{a}_1 f_0 \\ \bar{d}_2 \\ \bar{d}_3 \\ \vdots \\ \bar{d}_{N-1} - \bar{c}_{N-1} f_N \end{pmatrix} \end{aligned} \right\}. \quad (41)$$

The tridiagonal matrix  $A^*$  can be decomposed into the following form

$$A^* = LU, \quad (42)$$

where, L and U are respectively lower and upper triangular matrices and defined as

$$\left. \begin{aligned} L &= \begin{pmatrix} \beta_1 & 0 & 0 & & 0 \\ \bar{a}_2 & \beta_2 & 0 & & 0 \\ 0 & \bar{a}_3 & \beta_3 & \cdots & 0 \\ & \vdots & & \ddots & \vdots \\ 0 & 0 & 0 & \cdots & \beta_{N-1} \end{pmatrix} \\ U &= \begin{pmatrix} 1 & \gamma_1 & 0 & & 0 \\ 0 & 1 & \gamma_2 & & 0 \\ 0 & 0 & 1 & \cdots & 0 \\ & \vdots & & \ddots & \vdots \\ 0 & 0 & 0 & \cdots & 1 \end{pmatrix} \end{aligned} \right\}. \quad (43)$$

To find the unknowns  $(\beta_j, \gamma_j)$ ,  $j = 1, 2, 3, \dots, N-1$ , Equation (39) is utilized and is to be related as

$$\left. \begin{aligned} \beta_1 &= \bar{b}_1 \\ \gamma_1 &= \frac{\bar{c}_1}{\beta_1} \\ \beta_j &= \bar{b}_j - \bar{a}_j \gamma_{j-1} \quad \& \quad \gamma_j = \frac{\bar{c}_j}{\beta_j} \quad \text{for } j = 2, 3, 4, \dots, N-2 \\ \beta_j &= \bar{b}_j - \bar{a}_j \gamma_{j-1}, \quad \text{for } j = N-1 \end{aligned} \right\}, \quad (44)$$

To solve the linear system defined in Equation (38), we have to solve

$$\left. \begin{aligned} L(U\bar{f}) &= \bar{s} \\ U\bar{f} &= \bar{Z} \\ L\bar{Z} &= \bar{s} \end{aligned} \right\}. \quad (45)$$

Using this  $L\bar{Z} = \bar{s}$ , we have

$$\left. \begin{aligned} z_1 &= \frac{\bar{s}_1}{\beta_1} \\ z_j &= \frac{\bar{s}_j - \bar{a}_j z_{j-1}}{\beta_j} \text{ for } j = 2, 3, 4, \dots, N-1 \end{aligned} \right\}. \quad (46)$$

Finally using  $U\bar{f} = \bar{Z}$ , we get

$$\left. \begin{aligned} f_{N-1} &= z_{N-1} \\ f_j &= z_j - \gamma_j f_{j+1}, \text{ for } j = N-2, N-3, \dots, 2, 1 \end{aligned} \right\}. \quad (47)$$

Which is the solution of Equation (21).  $F$  can easily find from  $F' = f$ . This discretized form is expressed as

$$F_{j+1} = F_j + hf_j, \quad \text{for } j = 1 \quad \text{to } N \quad \text{with } F_1 = 0. \quad (48)$$

A similar procedure is followed for the solution of  $G$  and  $\Theta$ .

## 5. Results and discussion

The non-dimensional dynamical system of equations indicates that the thermal flow depends on five parameters ( $\alpha = 0.1, 0.3, 0.6, 0.8, 0.9$ ,  $Ec = 1.0, 2.0, 3.0, 4.0, 5.0$ ,  $Pr = 1.0, 2.0, 3.0, 4.0, 6.7$ ,  $\tau = 0.0, 0.5, 1.0, 1.5, 2.0$  and  $\lambda = 0.0, 1.0, 2.0, 3.5, 5.5$ ). The sixth parameter i.e. temperature difference parameter ( $\Lambda = 1.0, 2.0, 3.0, 4.0, 5.0$ ) appears in the dimensionless form of entropy production. The objective of the present section is to analyze the effects of mentioned parameters on  $F'(\xi)$ ,  $G'(\xi)$ ,  $N_G(\xi)$  and  $Be(\xi)$ . This objective is achieved by plotting the graphs of  $F'(\xi)$ ,  $G'(\xi)$ ,  $N_G(\xi)$  and  $Be(\xi)$  against the similarity variable ( $\xi$ ) and changing one of the concern parameters. To ensure the validation of the present numerical simulation, it is necessary to obtain numerical results for the special case of our problem already existing in the literature. Table 1 lists the existing numerical values in the literature as well as the numerical values obtained by FDM for this purpose. The excellent consistency between the values validates our numerical simulation. The numerical values of shear stresses and heat transfer rate at the boundary are computed against various combinations of key parameters and tabulated in Table 2. Further, the SLR technique is used to estimate the rate of decrease/increase in shear stresses and heat transfer rate at the boundary. It is found that  $-F''(0)$  is increasing function of  $Pr$  and  $\alpha$ , while decreasing behavior is observed with  $\tau$ ,  $\lambda$  and  $Ec$ . It is also found that the effects of  $Pr$ ,  $\tau$  and  $Ec$  on  $-F''(0)$  is relatively small. It is observed from Table 2 that  $-G''(0)$  rises with  $\lambda$ ,  $\tau$ ,  $\alpha$  and decreases with  $Pr$  and  $Ec$ . Relatively small effects of  $Pr$ ,  $\tau$  and  $Ec$  on  $-G''(0)$  is observed.  $-\Theta'(0)$  is directly proportional to the parameters  $Pr$ ,  $\lambda$  and  $\alpha$  while opposite effects are observed with the increasing values of parameters  $Ec$  and  $\tau$ . A comparatively little effect is observed on the heat transfer rate at the boundary. The slope linear regression (SLR) technique is used to compare the numerical values of heat transfer rate at the boundary in the presence and absence of viscous dissipation. Tables 3 and 4 demonstrate the numerical values of the heat transfer rate in the presence and absence of viscous dissipation, respectively. The SLR values show that an increase in

**Table 1.** Comparison of the numerical values of  $-\frac{d^2F}{d\xi^2}|_{\xi=0}$  and  $-\frac{d^2G}{d\xi^2}|_{\xi=0}$  obtained by SFDM with the existing values in the literature for  $Ec = 0$ ,  $\lambda = 0$  and  $\tau = 0$ .

$\alpha$	$-\frac{d^2F}{d\xi^2} _{\xi=0}$		$-\frac{d^2G}{d\xi^2} _{\xi=0}$	
	Liu et al. [45] Ackroyd Method and Runge-Kutta Integrating Scheme	Present Results SFDM	Liu et al. [45] Ackroyd Method and Runge-Kutta Integrating Scheme	Present Results SFDM
0.0	1.28180856	1.28180855	0.00000000	0.00000000
0.5	1.56988846	1.569888457	0.78494423	0.78494422
1.0	1.81275105	1.812751047	1.81275105	1.812751047

**Table 2.** Numerical estimation of  $-\frac{d^2F}{d\xi^2}|_{\xi=0}$ ,  $-\frac{d^2G}{d\xi^2}|_{\xi=0}$  and  $-\frac{d\Theta}{d\xi}|_{\xi=0}$  for assorted values of the important flow parameters.

$\tau$	Pr	$\alpha$	$\lambda$	$Ec$	SFDM		
					$-\frac{d^2F}{d\xi^2} _{\xi=0}$	$-\frac{d^2G}{d\xi^2} _{\xi=0}$	$-\frac{d\Theta}{d\xi} _{\xi=0}$
0					1.03458973	0.62753901	3.63122779
0.5					0.98359993	0.63064172	2.80951200
1.0	3.0	0.4	1.2	0.5	0.94103896	0.63353831	2.36096693
1.5					0.90432935	0.63625092	2.07081898
2.0					0.87198514	0.63879730	1.86427166
<b>Slope (Linear Regression)</b>					<b>-0.080895952</b>	<b>0.005625156</b>	<b>-0.854521056</b>
0.3	1.0				0.78477466	0.64941276	1.76535132
	2.0				0.92918096	0.63561445	2.50691835
	3.0	0.4	1.2	0.5	1.00277918	0.62942680	3.07069976
	4.0				1.04926986	0.62594224	3.54287878
	6.7				1.12097969	0.62130710	4.57199083
<b>Slope (Linear Regression)</b>					<b>0.05423763</b>	<b>-0.004428663</b>	<b>0.47959181</b>
0.3	3.0	0.1			0.80128621	0.14190497	2.82515136
		0.3			0.93939944	0.45696303	3.00136576
		0.6	1.2	0.5	1.11948896	1.00260204	3.16943571
		0.8			1.22429971	1.41146638	3.21157501
		0.9			1.27273401	1.62860441	3.21014407
<b>Slope (Linear Regression)</b>					<b>0.58772059</b>	<b>1.861339944</b>	<b>0.48104675</b>
0.3	3.0	0.4	0.0		1.51665633	0.60666253	2.85760221
			1.0		1.08533592	0.62597116	3.04059673
			2.0	0.5	0.68163910	0.64229682	3.17419285
			3.5		0.10853407	0.66345008	3.30961288
			5.5		0.61806774	0.68776888	3.40003374
<b>Slope (Linear Regression)</b>					<b>-0.18164191</b>	<b>0.014578085</b>	<b>0.09603855</b>
0.3	3.0	0.4		1.0	0.95280527	0.63416176	2.79792591
				2.0	0.866740096	0.64235094	2.34751881
				3.0	0.79525892	0.64917848	1.98823531
				4.0	0.73503912	0.65492792	1.69063755
				5.0	0.68368256	0.65980164	1.43512038
<b>Slope (Linear Regression)</b>					<b>-0.06699464</b>	<b>0.006385674</b>	<b>-0.338249232</b>

**Table 3.** Effects of mixed convection on  $-\frac{d\Theta}{d\xi}|_{\xi=0}$  in the absence of viscous dissipation.

$\lambda$	$-\frac{d\Theta}{d\xi} _{\xi=0}$
0	3.33096308
1	3.37685461
2	3.41793902
3.5	3.47309727
5.5	3.53797542
<b>SLR</b>	<b>0.03738221</b>

**Table 4.** Effects of mixed convection on  $-\frac{d\Theta}{d\xi}\big|_{\xi=0}$  in the presence of viscous dissipation.

$\lambda$	$-\frac{d\Theta}{d\xi}\big _{\xi=0}$
0	2.38257610
1	2.74234226
2	2.98044048
3.5	3.19057217
5.5	3.27579488
SLR	0.15587997

heat transfer rate with mixed convection parameter dominates in the presence of viscous dissipation.

It is shown in [Figure 2\(a\)](#) that the axial velocity  $F'(\xi)$  increases with the mixed convection parameter ( $\lambda$ ). Physically, a rise in mixed convection parameter leads to an increase in the buoyant force, which in turn leads to an augmentation of the axial velocity profile. As  $\lambda$  grows, a decrement in velocity  $G'(\xi)$  and temperature profile  $\Theta(\xi)$  is observed. This fact is depicted in [Figure 2\(b\)](#) and [\(c\)](#) respectively. In point of fact, as the values of the mixed-convection parameter in the flow region are increased, the buoyant forces begin to dominate the inertial forces. This results in an increase in the rate of heat transfer. As a direct consequence of this, a temperature profile and the thickness of its boundary layer turn out to be decreasing. It is noticed from [Figure 2\(d\)](#) that the rate of entropy generation  $N_G(\xi)$  is decreasing function of  $\lambda$  at the surface of the boundary and its vicinity. Physically, the axial velocity gradients are reduced with  $\lambda$  at the surface of the stretching boundary and adjacent to its vicinity. Since the formation of entropy is directly related to the velocity gradients, therefore, entropy generation  $N_G(\xi)$  is reduced at the surface of the stretching sheet and its proximity. In addition, it has been observed that after a predetermined amount of vertical distance ( $\xi$ ), an increase in the values of  $\lambda$  also causes an increase in the value of entropy generation. [Figure 2\(e\)](#) illustrates that the heat transfer effects are substantial as compared to friction heating irreversibility at the surface of the boundary for  $\lambda > 0$ . The thermal and viscous irreversibilities contribute equally at the boundary when  $\lambda = 0$ . Further, after a certain value of the vertical distance from the surface of the stretching sheet, the Bejan number decreases with growing values of  $\lambda$ . It is also clearly seen that the viscous effect is prominent throughout the flow region after a certain value of  $\xi$ .

[Figure 3\(a\)–\(c\)](#) respectively indicate the influence of the thermal conductivity parameter ( $\tau$ ) on  $\Theta(\xi)$ ,  $N_G(\xi)$  and Bejan number ( $Be(\xi)$ ). The temperature  $\Theta(\xi)$  rises as  $\tau$  enhanced. This is because the fluid's capacity for thermal conduction increases with increasing values of  $\tau$ , leading to an increase in the fluid's temperature. The entropic generation increases as  $\tau$  increases but this increasing effect can be seen after a specific vertical distance from the stretching boundary. The graph of  $Be(\xi)$  against  $\xi$  is plotted by taking different values of  $\tau$ . It is observed from this plot that  $Be(\xi)$  increases as  $\tau$  increases. Further, the effects are not very much prominent at the surface of the boundary. Heat transfer irreversibility is dominant over frictional heating irreversibility at the boundary.

[Figure 4\(a\)](#) showed that as the values of the Pr number increased, the temperature of the fluid decreased continuously. The reason for this is that the thickness of the thermal boundary layer and the Pr number has an inverse relationship. [Figure 4\(b\)](#) displays that the rate of entropy generation  $N_G(\xi)$  enhances as the Prandtl number Pr increases. On a physical basis, this behavior can be explained as, since entropy is increasing function of thermal gradients and thermal gradients increases with Pr number so consequently entropy rises with rising values of Pr number. The graph of the Bejan number is plotted for various values of the Prandtl number as shown in [Figure 4\(c\)](#). It is perceived that the Bejan number declines as Pr rises. Further, the values of the Bejan number at the surface of the boundary and its neighborhood show that thermal transfer

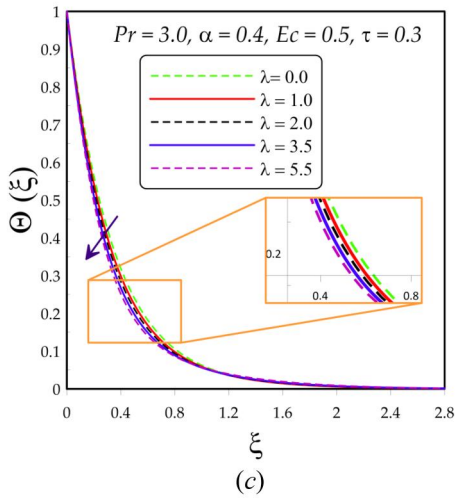
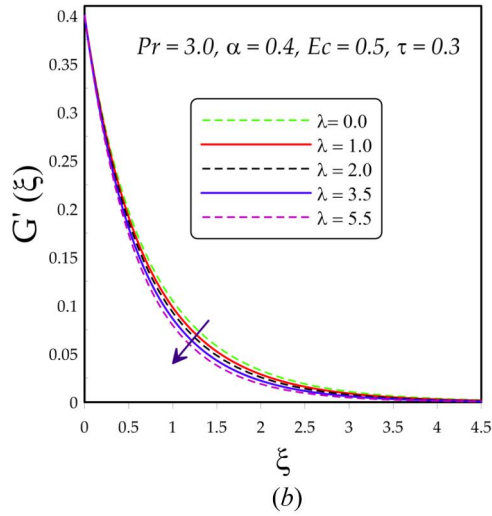
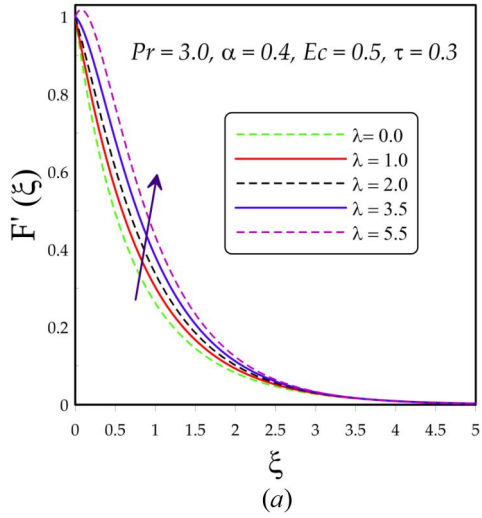


Figure 2. Effects of  $\lambda$  on (a)  $F'(\xi)$  (b)  $G'(\xi)$  (c)  $\Theta(\xi)$  (d)  $N_G(\xi)$  (e)  $Be(\xi)$ .

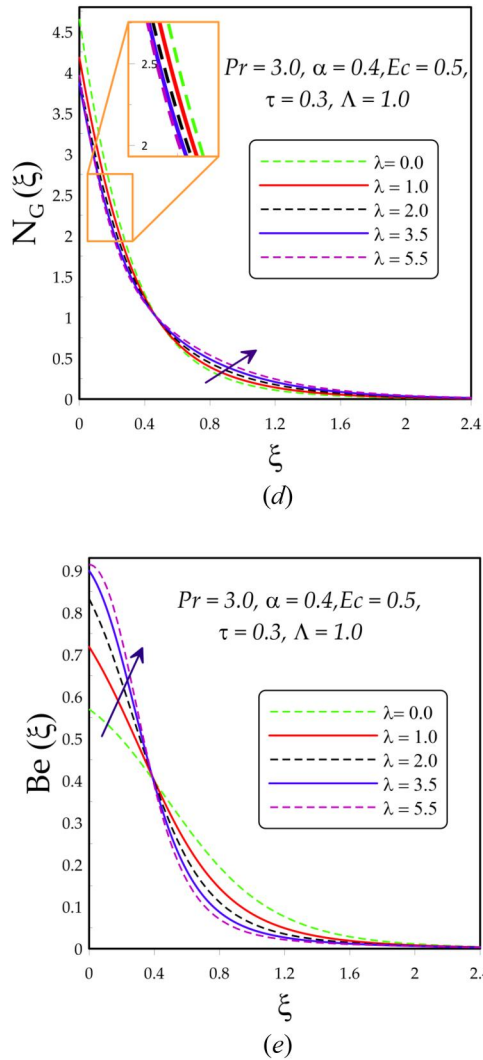


Figure 2. Continued

effects are dominant in this region whereas the thermal effects are less significant in the region away from the stretching boundary.

Figure 5(a) illustrates the thickening of the thermal boundary layer with increasing values of Eckert number. This characteristic can be described physically as, since the Eckert number is a measurement of the kinetic energy that transforms into heat energy as a result of frictional forces between the fluid layers, therefore a temperature rise is noticed with an increase in  $Ec$ . Since dissipative energy is directly related to the Eckert number and dissipative energy is also a source of entropy generation, therefore entropy generation enhances with the Eckert number as shown in Figure 5(b). The graph of the Bejan number ( $Be(\xi)$ ) for specific values of the Eckert number against  $\xi$  is plotted in Figure 5(c). A decline in the Bejan number is found with rising values of  $Ec$ . Figure 6(a) and (b) respectively represent the effects of the stretching ratio parameter ( $\alpha$ ) on  $F'(\xi)$  and  $G'(\xi)$ . A decrement in  $F'(\xi)$  increment in  $G'(\xi)$  is examined with rising values of  $\alpha$ . This is due to the fact that increasing values of  $\alpha$  indicate a decrease in stretching

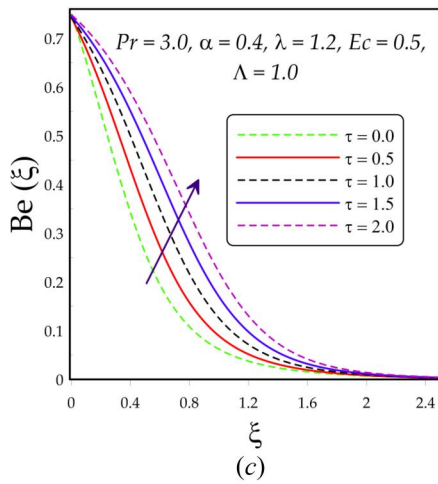
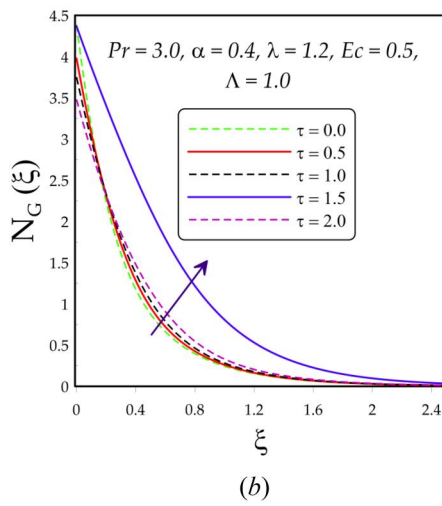
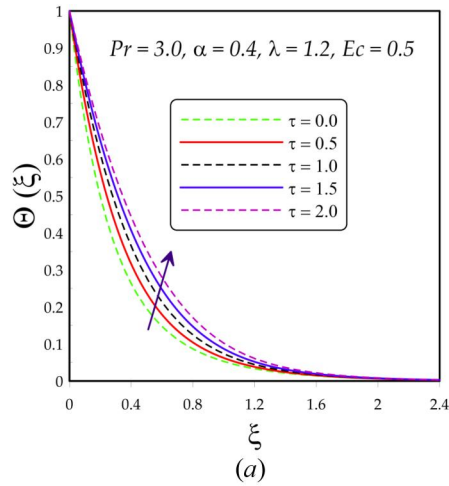


Figure 3. Effects of  $\tau$  on (a)  $\Theta(\xi)$  (b)  $N_G(\xi)$  (c)  $Be(\xi)$ .

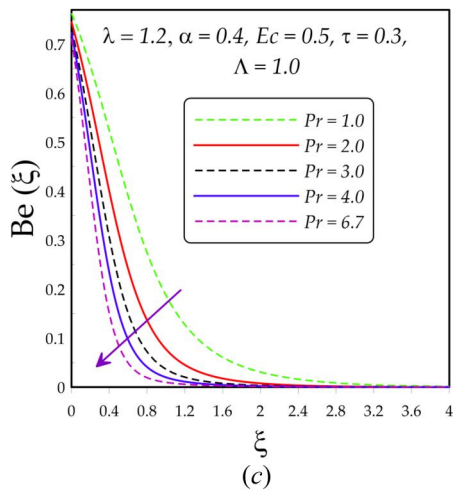
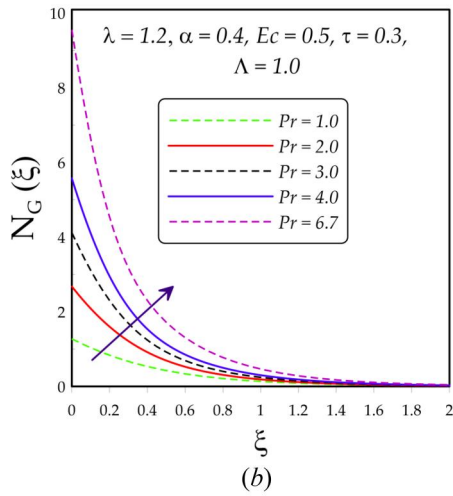
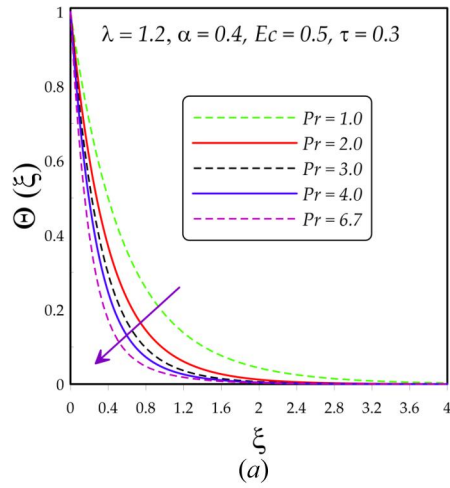


Figure 4. Effects of Pr on (a)  $\Theta(\xi)$  (b)  $N_G(\xi)$  (c)  $Be(\xi)$ .

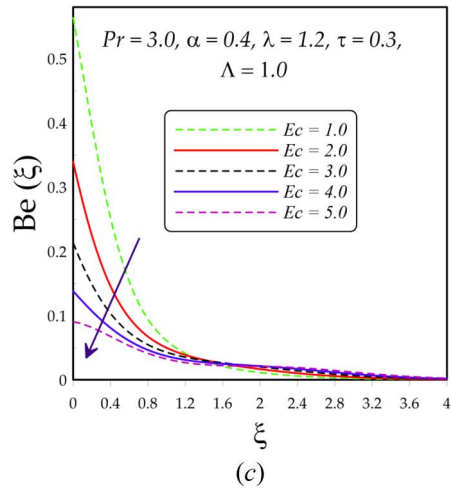
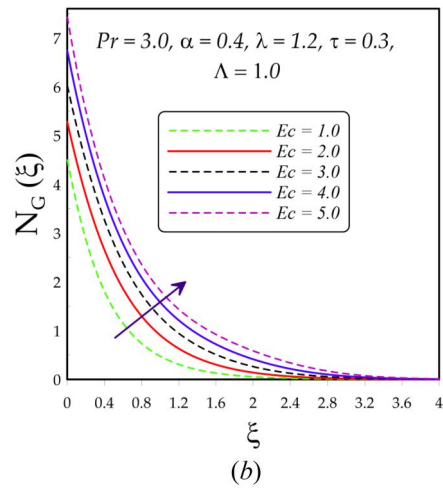
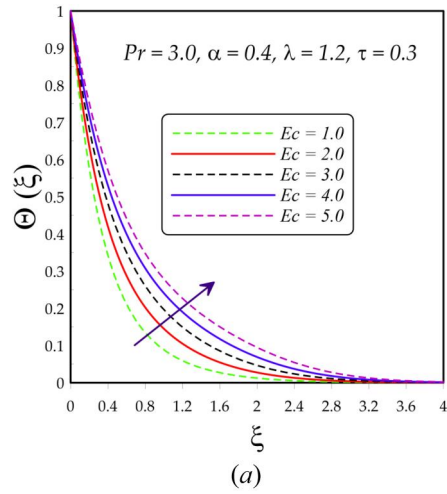


Figure 5. Effects of  $Ec$  on (a)  $\Theta(\xi)$  (b)  $N_G(\xi)$  (c)  $Be(\xi)$ .

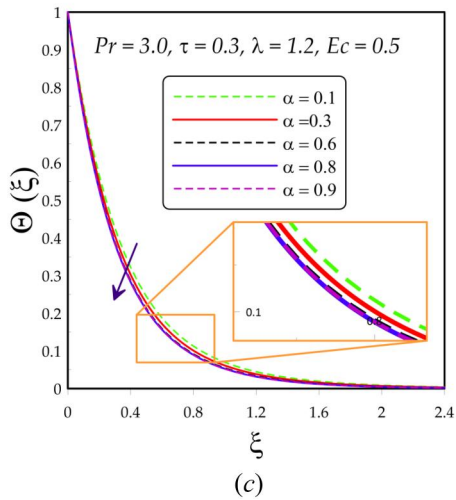
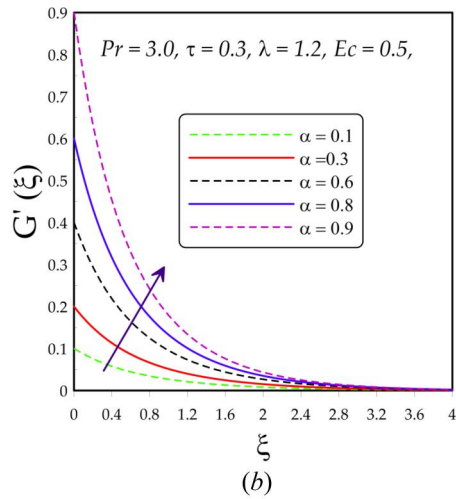
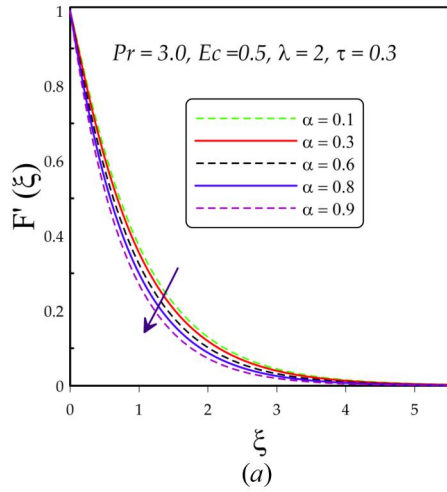


Figure 6. Effects of  $\alpha$  on (a)  $F'(\xi)$  (b)  $G'(\xi)$  (c)  $\Theta(\xi)$  (d)  $N_G(\xi)$  (e)  $Be(\xi)$ .

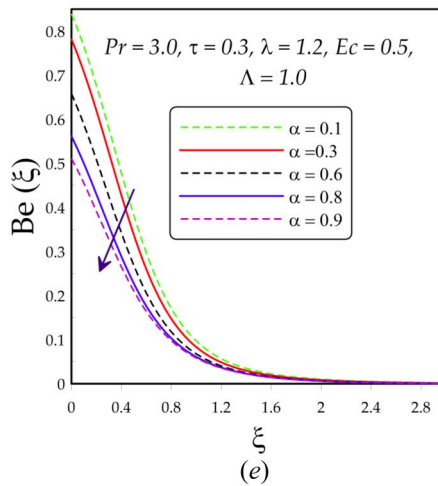
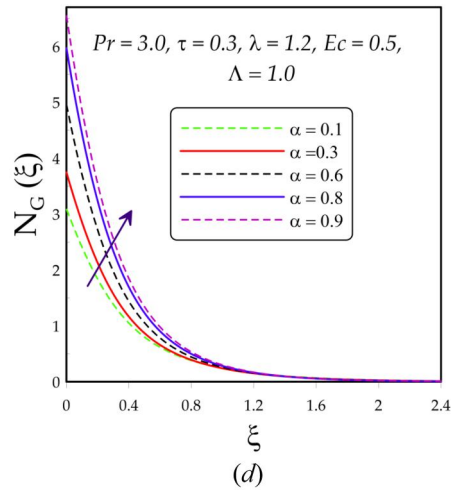


Figure 6. Continued

velocity in the  $x^*$ -direction, which, as a consequence, results in a decrease in axial velocity. On a more fundamental level, as  $\alpha$  increases, the stretching rate along the  $y^*$ -axis also increases, which causes the fluid to accelerate in the direction of the  $y$ -axis. Figure 6(c) shows a direct relation between entropy generation and  $(\alpha)$ . In other words, entropy generation can be minimized by increasing the stretching rate along  $x^*$  – axis or by reducing the stretching rate alongside  $y^*$  – axis. The contribution of viscous dissipation in entropy generation is increasing function of  $\alpha$  and this relation can be seen in Figure 6(d). The temperature difference parameter ( $\Lambda$ ) is the key factor to analyze the entropy generation within the boundary layer and this parameter appears during the non-dimensionalization of the volumetric rate of entropy generation. It is found that the profile of entropy generation  $N_G(\xi)$  and Bejan number decline as  $\Lambda$  increases as shown in Figure 7(a) and (b) respectively. This characteristic can be physically described as follows: since the temperature difference parameter increases with decreasing the operating temperature difference, this reduction causes less heat transfer and, as a result, the entropy generation decreases because entropy generation decreases with decreasing heat transfer.

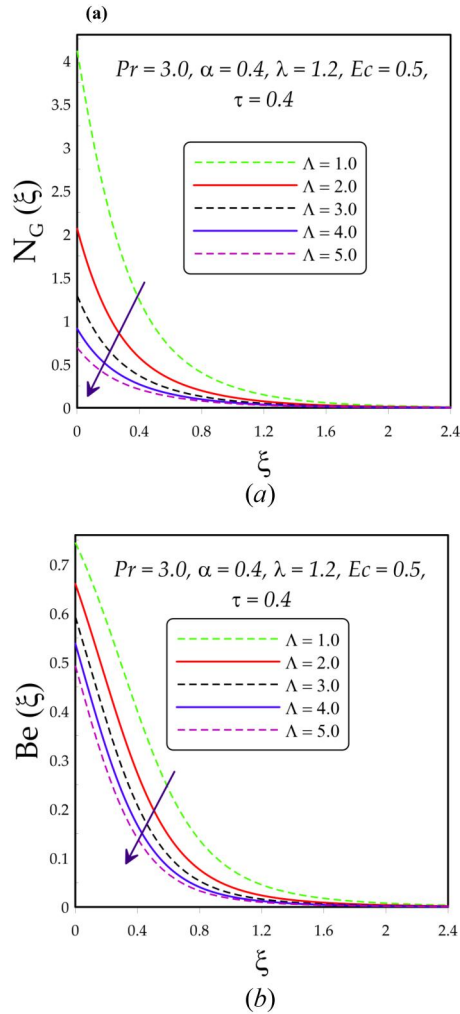


Figure 7. Effects of  $\Lambda$  on (a)  $N_G(\xi)$  (b)  $Be(\xi)$ .

## 6. Concluding remarks

The current study gives the results of a three-dimensional mixed convection flow of dissipative fluid with thermal conductivity and analysis of entropy generation. The numerical solutions of the dimensionless governing equations are obtained by the implementation of the simplified finite difference method (SFDM). The key findings of the current study and future research direction are as follows:

- Axial velocity  $F'(\xi)$  increases with the mixed convection parameter ( $\lambda$ ) while decrement in velocity  $G'(\xi)$  and temperature profile  $\Theta(\xi)$  is observed.
- The rate of entropy generation  $N_G(\xi)$  is decreasing function of  $\lambda$  at the surface of the boundary and its vicinity.
- The temperature  $\Theta(\xi)$  and  $Be(\xi)$  rises as  $\tau$  enhanced. The entropy generation increases as  $\tau$  increases but this increasing effect can be seen after a specific vertical distance from the stretching boundary.
- Increasing the Prandtl number decelerates the fluid and weakens the momentum boundary layer.

- The rate of entropy generation  $N_G(\zeta)$  enhances as the Prandtl number (Pr) increases.
- The thickening of the thermal boundary layer is observed with increasing Eckert number.
- The rate of entropy generation  $N_G(\zeta)$  enhances as the Eckert number ( $Ec$ ) increases while opposite effects on the Bejan number are observed.

## 7. Future work

The mathematical model becomes locally non-similar in the case of temperature-dependent viscosity and can be studied in future. Most of the authors treat it as self-similar but treating the local nonsimilar problems as self-similar produces inaccurate results. Additionally, the second law analysis of time-dependent three-dimensional flow along with nanoparticle effects can be studied in the future, which will also be of great interest. This study is important because of the various industrial and engineering applications of nanofluids such as cooling processes, microelectromechanical systems, implantable nanotherapeutic devices, cancer therapy, etc.

## Disclosure statement

No potential conflict of interest was reported by the authors.

## ORCID

Muhammad Idrees Afridi  <http://orcid.org/0000-0002-8818-5980>

Ali J. Chamkha  <http://orcid.org/0000-0002-8335-3121>

## References

- [1] A. Bejan, *Entropy Generation through Heat and Fluid Flow*, Wiley, New York, 1982.
- [2] A. Bejan, "Entropy generation minimization: the new thermodynamics of finite-size devices and finite-time processes," *J. Appl. Phys.*, vol. 79, no. 3, pp. 1191–1218, 1996. Feb DOI: [10.1063/1.362674](https://doi.org/10.1063/1.362674).
- [3] S. Mahmud and R. A. Fraser, "Flow, thermal, and entropy generation characteristics inside a porous channel with viscous dissipation," *Int. J. Therm.*, vol. 44, no. 1, pp. 21–32, 2005. Jan DOI: [10.1016/j.ijthermalsci.2004.05.001](https://doi.org/10.1016/j.ijthermalsci.2004.05.001).
- [4] T. H. Ko, "Numerical analysis of entropy generation and optimal Reynolds number for developing laminar forced convection in double-sine ducts with various aspect ratios," *Int. J. Heat Mass Transf.*, vol. 49, no. 3–4, pp. 718–726, 2006. Feb DOI: [10.1016/j.ijheatmasstransfer.2005.08.023](https://doi.org/10.1016/j.ijheatmasstransfer.2005.08.023).
- [5] O. D. Makinde and A. S. Eegunjobi, "Effects of Convective Heating on Entropy generation rate in a channel with permeable walls," *Entropy*, vol. 15, no. 1, pp. 220–233, 2013. Jan DOI: [10.3390/e15010220](https://doi.org/10.3390/e15010220).
- [6] M. M. Rashidi, M. M. Bhatti, M. A. Abbas and M. E. S. Ali, "Entropy generation on MHD blood flow of nanofluid due to peristaltic waves," *Entropy*, vol. 18, no. 4, pp. 117–123, 2016. Apr DOI: [10.3390/e18040117](https://doi.org/10.3390/e18040117).
- [7] M. M. Bhatti and M. M. Rashidi, "Numerical simulation of entropy generation on MHD nanofluid towards a stagnation point flow over a stretching surface," *Int. J. Appl. Comput. Math.*, vol. 3, no. 3, pp. 2275–2289, 2017. Jun DOI: [10.1007/s40819-016-0193-4](https://doi.org/10.1007/s40819-016-0193-4).
- [8] T. Armaghani, A. Kasaeipoor, N. Alavi and M. M. Rashidi, "Numerical investigation of water-alumina nanofluid natural convection heat transfer and entropy generation in a baffled L-shaped cavity," *J. Mol. Liq.*, vol. 223, pp. 243–251, 2016. Nov DOI: [10.1016/j.molliq.2016.07.103](https://doi.org/10.1016/j.molliq.2016.07.103).
- [9] M. I. Afridi and M. Qasim, "Second law analysis of Blasius flow with nonlinear Rosseland thermal radiation in the presence of viscous dissipation," *Propuls. Power Res.*, vol. 8, no. 3, pp. 234–242, 2019. Sep DOI: [10.1016/j.jprr.2018.06.001](https://doi.org/10.1016/j.jprr.2018.06.001).
- [10] P. B. A. Reddy, T. Salah, S. Jakeer, M. A. Mansour and A. M. Rashad, "Entropy generation due to magneto-natural convection in a square enclosure with heated corners saturated porous medium using Cu/water nanofluid," *Chi. J. Phys.*, vol. 77, pp. 1863–1884, 2022. Jun DOI: [10.1016/j.cjph.2022.01.012](https://doi.org/10.1016/j.cjph.2022.01.012).
- [11] M. Qasim, Z. Ali, U. Farooq and D. C. Lu, "Investigation of entropy in two-dimensional peristaltic flow with temperature dependent viscosity, thermal and electrical conductivity," *Entropy*, vol. 22, no. 2, pp. 200, 2020. Feb DOI: [10.3390/e22020200](https://doi.org/10.3390/e22020200).

- [12] Z. Ali, M. Qasim and M. U. Ashraf, "Thermodynamic analysis of nonlinear convection in peristaltic flow," *Int. Commun. Heat Mass Transf.*, vol. 129, pp. 105686, Dec. 2021. DOI: [10.1016/j.icheatmasstransfer.2021.105686](https://doi.org/10.1016/j.icheatmasstransfer.2021.105686).
- [13] H. Schlichting and K. Gersten, *Boundary-Layer Theory*, 2003, Berlin Heidelberg: Springer Science & Business Media.
- [14] Aamir, Hamid, Masood, Khan, Abdul, Hafeez, Hashim, "Unsteady stagnation-point flow of Williamson fluid generated by stretching/shrinking sheet with Ohmic heating," *Int. J. Heat Mass Transf.*, vol. 126, pp. 933–940, Nov. 2018. DOI: [10.1016/j.ijheatmasstransfer.2018.05.076](https://doi.org/10.1016/j.ijheatmasstransfer.2018.05.076).
- [15] M. V. Krishna, N. A. Ahammad and E. A. Algehyne, "Unsteady MHD third-grade fluid past an absorbent high-temperature shrinking sheet packed with silver nanoparticles and non-linear radiation," *J. Taibah Univ. Sci.*, vol. 16, no. 1, pp. 585–593, 2022. Jun DOI: [10.1080/16583655.2022.2087396](https://doi.org/10.1080/16583655.2022.2087396).
- [16] R. J. P. Gowda, A. Rauf, R. Naveen Kumar, B. C. Prasannakumara and S. A. Shehzad, "Slip flow of Casson-Maxwell nanofluid confined through stretchable disks," *Indian J. Phys.*, vol. 96, no. 7, pp. 2041–2049, 2022. Jun DOI: [10.1007/s12648-021-02153-7](https://doi.org/10.1007/s12648-021-02153-7).
- [17] M. V. Krishna, "Thermodiffusion, chemical reaction, and Hall and ion-slip impacts on MHD rotating flow past an infinite vertical porous plate," *Heat Trans.*, vol. 50, no. 8, pp. 8426–8452, 2021. Jun DOI: [10.1002/hjt.22283](https://doi.org/10.1002/hjt.22283).
- [18] M. Israr Ur Rehman, *et al.*, "Soret and Dufour influences on forced convection of Cross radiative nanofluid flowing via a thin movable needle," *Sci. Rep.*, vol. 12, no. 1, pp. 18666, 2022. Nov DOI: [10.1038/s41598-022-23563-5](https://doi.org/10.1038/s41598-022-23563-5).
- [19] R. J. P. Gowda, *et al.*, "Dynamics of nanoparticle diameter and interfacial layer on flow of non-Newtonian (Jeffrey) nanofluid over a convective curved stretching sheet," *Int. J. Mod. Phys. B*, vol. 36, no. 31, pp. 2250224, 2022. Aug. DOI: [10.1142/S0217979222502241](https://doi.org/10.1142/S0217979222502241).
- [20] F. Wang, S. P. Rani, K. Sarada, R. J. Punith Gowda, U. Khan, H. Y. Zahran and E. E. Mahmoud, "The effects of nanoparticle aggregation and radiation on the flow of nanofluid between the gap of a disk and cone," *Case Stud. Therm. Eng.*, vol. 33, pp. 101930, May. 2022. DOI: [10.1016/j.csite.2022.101930](https://doi.org/10.1016/j.csite.2022.101930).
- [21] T. Hayat, M. Qasim and Z. Abbas, "Homotopy solution for the unsteady three-dimensional MHD flow and mass transfer in a porous space," *Commun. Nonlinear Sci. Numer. Simul.*, vol. 15, no. 9, pp. 2375–2387, 2010. Sep DOI: [10.1016/j.cnsns.2009.09.013](https://doi.org/10.1016/j.cnsns.2009.09.013).
- [22] M. Qasim, "Heat and mass transfer in a Jeffrey fluid over a stretching sheet with heat source/sink," *Alex. Eng. J.*, vol. 52, no. 4, pp. 571–575, 2013. Dec DOI: [10.1016/j.aej.2013.08.004](https://doi.org/10.1016/j.aej.2013.08.004).
- [23] S. Mosayebidorcheh, O. D. Makinde, D. D. Ganji and M. A. Chermahini, "DTM-FDM hybrid approach to unsteady MHD Couette flow and heat transfer of dusty fluid with variable properties," *Therm. Sci. Eng. Prog.*, vol. 2, pp. 57–63, 2017. Jun DOI: [10.1016/j.tsep.2017.04.003](https://doi.org/10.1016/j.tsep.2017.04.003).
- [24] Masood, Khan, Aamir, Hamid, Hashim, "Numerical investigation on time-dependent flow of Williamson nanofluid along with heat and mass transfer characteristics past a wedge geometry," *Int. J. Heat Mass Transf.*, vol. 118, pp. 480–491, Mar. 2018. DOI: [10.1016/j.ijheatmasstransfer.2017.10.126](https://doi.org/10.1016/j.ijheatmasstransfer.2017.10.126).
- [25] M. Qasim, M. I. Afridi, A. Wakif and S. Saleem, "Influence of variable transport properties on nonlinear radioactive Jeffrey fluid flow over a disk: utilization of generalized differential quadrature method," *Arab. J. Sci. Eng.*, vol. 44, no. 6, pp. 5987–5996, 2019. Mar DOI: [10.1007/s13369-019-03804-y](https://doi.org/10.1007/s13369-019-03804-y).
- [26] Q.-H. Shi, *et al.*, "Numerical study of bio-convection flow of magneto-cross nanofluid containing gyrotactic microorganisms with activation energy," *Sci. Rep.*, vol. 11, no. 1, pp. 16030, 2021. Aug DOI: [10.1038/s41598-021-95587-2](https://doi.org/10.1038/s41598-021-95587-2).
- [27] Y. Yang, M. Israr Ur Rehman, A. Hamid and S. Ullah, "Multiple solutions for stagnation-point flow of unsteady Carreau fluid along a permeable stretching/shrinking sheet with non-uniform heat generation," *Coatings*, vol. 11, no. 9, pp. 1012, 2021. Aug. DOI: [10.3390/coatings11091012](https://doi.org/10.3390/coatings11091012).
- [28] X. Zhang, D. Yang, M. Israr Ur Rehman, A. A. Mousa and A. Hamid, "Numerical simulation of bioconvection radiative flow of Williamson nanofluid past a vertical stretching cylinder with activation energy and swimming microorganisms," *Case Stud. Therm. Eng.*, vol. 33, pp. 101977, 2022. May. 101977. DOI: [10.1016/j.csite](https://doi.org/10.1016/j.csite).
- [29] R. N. Kumar, F. Gamaoun, A. Abdulrahman, J. Singh Chohan and R. J. P. Gowda, "Heat transfer analysis in three-dimensional unsteady magnetic fluid flow of water-based ternary hybrid nanofluid conveying three various shaped nanoparticles: a comparative study," *Int. J. Mod. Phys. B*, vol. 36, no. 25, pp. 2250170, July. 2022. DOI: [10.1142/S0217979222501703](https://doi.org/10.1142/S0217979222501703).
- [30] J. C. Umavathi, *et al.*, "Magnetohydrodynamic squeezing Casson nanofluid flow between parallel convectively heated disks," *Int. J. Mod. Phys. B*, vol. 37, no. 04, pp. 2350031, 2023. Sep. DOI: [10.1142/S0217979223500315](https://doi.org/10.1142/S0217979223500315).
- [31] A. Nakayama, H. Koyama and S. Ohsawa, "Self-similar thermal boundary layers on plane and axisymmetric bodies," *Wärme - Und Stoffübertragung*, vol. 18, no. 2, pp. 69–73, 1984. Jun DOI: [10.1007/BF01006601](https://doi.org/10.1007/BF01006601).
- [32] A. Mehmood, *Viscous Flows: Stretching and Shrinking of Surfaces*, 2017, Switzerland: Springer.

- [33] J. Merkin, I. Pop, Y. Y. Lok and T. Grosan, "Similarity Solutions for the Boundary Layer Flow and Heat Transfer of Viscous Fluids," *Nanofluids, Porous Media, and Micropolar Fluids*, 2021, Academic Press.
- [34] H. Thameem. Basha and R. Sivaraj, "Numerical simulation of blood nanofluid flow over three different geometries by means of gyrotactic microorganisms: applications to the flow in a circulatory system," *Proc. Inst. Mech. Eng. Part C*, vol. 235, no. 2, pp. 441–460, 2021. Jan DOI: [10.1177/0954406220947](https://doi.org/10.1177/0954406220947).
- [35] A. Ridha and M. Curie, "Aiding flows non-unique similarity solutions of mixed-convection boundary-layer equations," *Z. Angew. Math. Phys.* vol. 47, no. 3, pp. 341–352, May. 1996. DOI: [10.1007/BF00916642](https://doi.org/10.1007/BF00916642).
- [36] C. H. Chen, "Laminar mixed convection adjacent to vertical continuously stretching sheets," *Heat Mass Transf.*, vol. 33, no. 5-6, pp. 471–476, 1998. Apr DOI: [10.1007/s002310050217](https://doi.org/10.1007/s002310050217).
- [37] S. P. A. Devi and M. Prakash, "Temperature dependent viscosity and thermal conductivity effects on hydro-magnetic flow over a slendering stretching sheet," *J. Niger. Soc. Math.*, vol. 34, no. 3, pp. 318–330, 2015. Dec. 2015.07.002. DOI: [10.1016/j.jnnms](https://doi.org/10.1016/j.jnnms).
- [38] M. I. Afridi, M. Qasim and I. Khan, "Entropy generation minimization in MHD boundary layer flow over a slendering stretching sheet in the presence of frictional and Joule heating," *J. Korean Phys. Soc.*, vol. 73, no. 9, pp. 1303–1309, 2018. Nov DOI: [10.3938/jkps.73.1303](https://doi.org/10.3938/jkps.73.1303).
- [39] M. I. Afridi, M. Qasim, I. Khan, S. Shafie and A. S. Alshomrani, "Entropy generation in magnetohydrodynamic mixed convection flow over an inclined stretching sheet," *Entropy*, vol. 19, no. 1, pp. 10, 2016. Dec DOI: [10.3390/e19010010](https://doi.org/10.3390/e19010010).
- [40] M. Qasim, N. Riaz, D. C. Lu and M. I. Afridi, "Mixed convection flow over a stretching sheet of variable thickness: analytical and numerical solutions of self-similar equations," *Heat Trans.*, vol. 49, no. 6, pp. 3882–3899, 2020. Jun DOI: [10.1002/htj.21813](https://doi.org/10.1002/htj.21813).
- [41] M. K. Partha, P. V. S. N. Murthy, P. V. S. N and G. P. Rajasekhar, "Effect of viscous dissipation on the mixed convection heat transfer from an exponentially stretching surface," *Heat Mass Transf.*, vol. 41, no. 4, pp. 360–366, 2005. Sep DOI: [10.1007/s00231-004-0552-2](https://doi.org/10.1007/s00231-004-0552-2).
- [42] B. Bidin and R. Nazar, "Numerical solution of the boundary layer flow over an exponentially stretching sheet with thermal radiation," *Eur. J. Sci. Res.*, vol. 33, no. 4, pp. 710–717, 2009. BJul
- [43] M. I. Afridi, M. Qasim and O. D. Makinde, "Second law analysis of boundary layer flow with variable fluid properties," *J. Heat. Transf.*, vol. 139, no. 10, pp. 104505, 2017. Oct 2017 DOI: [10.1115/1.4036645](https://doi.org/10.1115/1.4036645).
- [44] M. Qasim and M. I. Afridi, "Effects of energy dissipation and variable thermal conductivity on entropy generation rate in mixed convection flow," *J. Therm. Sci. Eng. Appl.*, vol. 10, no. 4, pp. 044501, Aug. 2018. DOI: [10.1115/1.4038703](https://doi.org/10.1115/1.4038703).
- [45] I. C. Liu, H. H. Wang and Y. F. Peng, "Flow and heat transfer for three-dimensional flow over an exponentially stretching surface," *Chem. Eng. Commun.*, vol. 200, no. 2, pp. 253–268, 2013. Nov DOI: [10.1080/00986445.2012.703148](https://doi.org/10.1080/00986445.2012.703148).
- [46] M. I. Afridi and M. Qasim, "Entropy generation in three-dimensional flow of dissipative fluid," *Int. J. Appl. Comput. Math.*, vol. 4, no. 1, pp. 1–11, 2018. DOI: [10.1007/s40819-017-0454-x](https://doi.org/10.1007/s40819-017-0454-x).
- [47] T. Y. Na, *Computational Methods in Engineering Boundary Value Problems*, 1980, Academic Press, Cambridge, MA, USA.
- [48] M. Irfan, M. Asif Farooq, T. Iqra, A. Mushtaq and Z. H. Shamsi, "A simplified finite difference method (SFDM) for EMHD Powell–Eyring nanofluid flow featuring variable thickness surface and variable fluid characteristics," *Math. Probl. Eng.* vol. 2020, pp. 8823905, Nov. 2020. DOI: [10.1155/2020/8823905](https://doi.org/10.1155/2020/8823905).